CHEMISTRY OF MATERIALS

Article

pubs.acs.org/cm

Benzotriazole-Containing Planar Conjugated Polymers with Noncovalent Conformational Locks for Thermally Stable and Efficient Polymer Field-Effect Transistors

Seungjib Yum,[†,Δ] Tae Kyu An,[‡,Δ] Xiaowei Wang,[†,Δ] Wonho Lee,[†] Mohammad Afsar Uddin,[†] Yu Jin Kim,[‡] Thanh Luan Nguyen,[†] Shuhao Xu,[†] Sungu Hwang,[†] Chan Eon Park,*[,‡] and Han Young Woo*[,†]

[†]Department of Nanofusion Engineering, Department of Cogno-Mechatronics Engineering, Pusan National University, Miryang, Gyeongsangnam-do 627-706, Korea

[‡]POSTECH Organic Electronics Laboratory, Polymer Research Institute, Department of Chemical Engineering, Pohang University of Science and Technology, Pohang, North Gyeongsang 790-784, Korea

Supporting Information

ABSTRACT: We report a series of benzotriazole-based semicrystalline π-conjugated polymers with noncovalent conformational locks for applications in polymer field-effect transistors. The benzotriazole moiety is a versatile electron-deficient building block that offers two chemically functionalizable sites, 2(N) and 5, 6(C) positions, allowing easy modulation of the solution processability and electronic structures of the resulting polymers. Fluorine or alkoxy substituents were introduced to the benzotriazole unit to enhance the molecular ordering through intra- and intermolecular F···S, F···H−C, C−F···π_F, or S···O attractive interactions. The fluorinated polymer (**PTBTz-F**) showed remarkably enhanced hole mobility (μ_h = 1.9 cm^2/(V·s), on/off ratio = 8 × 10^7) upon thermal annealing at 305 °C, compared to the unsubstituted one (**PTBTz**) (μ_h = 7.0 × 10^{-3} cm^2/(V·s), on/off ratio = 3 × 10^6). Alkoxy unit substitution (**PTBTz-OR**) also improved the carrier mobility up to 0.019 cm^2/(V·s) with an on/off ratio of 4 × 10^5. Fluorine or alkoxy substitution induced tight interchain ordering with edge-on orientation, as confirmed by X-ray diffraction measurements. In particular, fluorinated **PTBTz-F** showed high thermal stability (T_d 453 °C) and the remarkable device characteristics with deep frontier orbital levels.

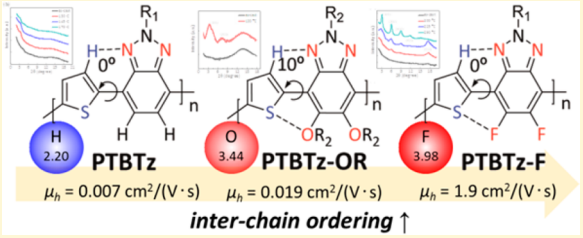

INTRODUCTION

Polymer field-effect transistors (PFETs) have been studied extensively because of their low-cost, large-area and solution processability, mechanical flexibility along with their potential applications in smart cards, radio frequency identification, and displays.[1−3] The molecular design and synthesis of conjugated polymers for effective charge transports are of prime importance to realize highly efficient PFETs.[4−6] Although conjugated polymers are suitable materials for easy device fabrication via a solution process, the carrier mobility of PFETs is limited because of the poor interchain packing of the polymers and macroscopic defects originating from the weak van der Waals forces among the adjacent polymers.[7] Favorable molecular ordering with high crystallinity is a key factor for realizing high performance PFETs. A number of D−A (donor−acceptor) type copolymers have been synthesized, realizing high hole mobility surpassing ∼1 cm^2/(V·s).[8−10] Incorporating appropriate structural moieties into the D−A copolymers can fine-tune the chain curvature, torsional angle, electronic structure of the polymer chains, and resulting intermolecular interactions, thereby affecting charge transport.[11] An alternating copolymer containing cyclopentadithiophene (CDT) as a donor unit and benzothiadiazole (BT) as an acceptor unit showed a hole mobility of ∼3 cm^2/(V·s).[4] The combination of diketopyrrolopyrrole (DPP) or isoindigo (IDG) units with a range of thiophene derivatives has attracted considerable attention because of their extremely high hole mobility of up to ∼12 cm^2/(V·s).[5,12,13] In addition to the high charge carrier mobility, thermal, oxidation, and temporal device stability should be also considered carefully for the design of ideal active materials for PFETs.

A benzotriazole moiety has been widely studied as an electron-deficient unit in D−A copolymers for photovoltaic applications, showing power conversion efficiencies (PCE) of up to ∼7%.[14−16] The benzotriazole unit offers two chemically functionalizable sites (Scheme 1). i) The central nitrogen position can be functionalized with an alkyl chain (to endow solution processability) separate from a conjugated backbone that reduces the steric hindrance, thereby enhancing the effective intrachain π-conjugation and interchain packing. ii) The 5- and 6-positions on the benzotriazole unit can be modified chemically by introducing other substituents[17] (i.e., alkoxy and fluorine groups, etc.), modulating the frontier orbital levels and oxidational stability of the resulting molecules. The

Received: December 29, 2013
Revised: February 21, 2014
Published: February 22, 2014

dx.doi.org/10.1021/cm4042346 | Chem. Mater. 2014, 26, 2147−2154

Scheme 1. (a) Synthetic Routes to BTz-Based Monomers and Polymers[a] and (b) Schematic Noncovalent Bonding in BTz Based Polymers

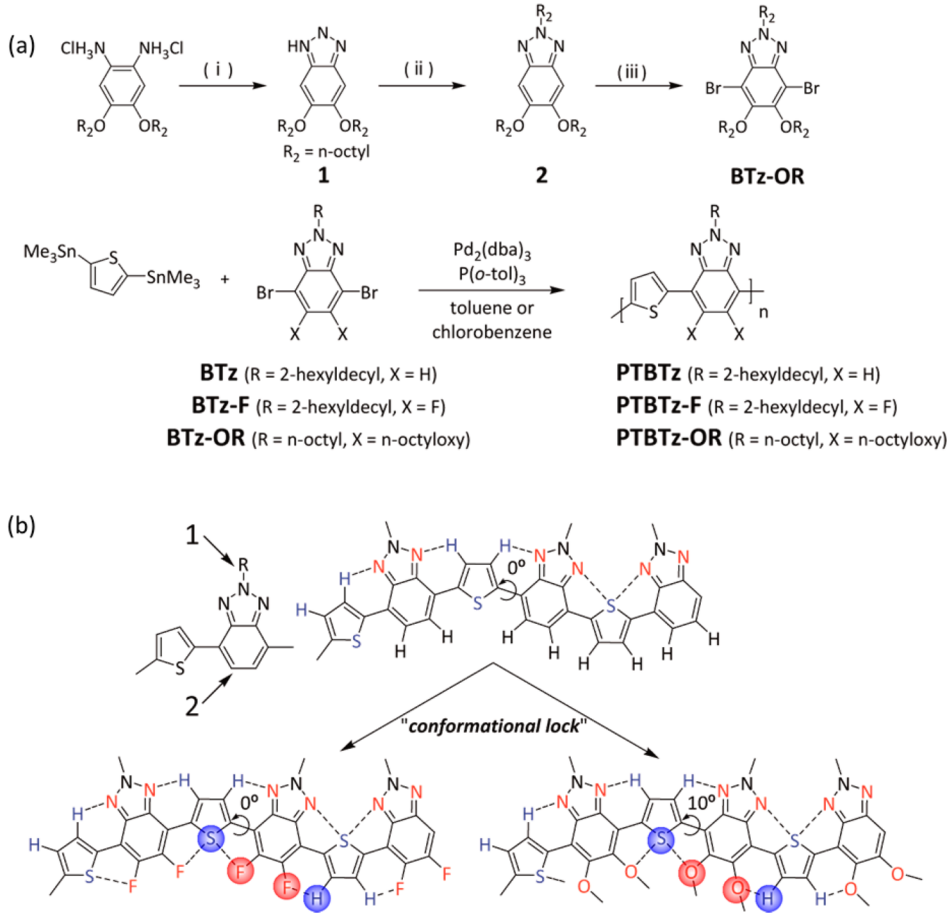

[a]Reagents and conditions: (i) $NaNO_2$, AcOH, H_2O; (ii) t-BuOK, 1-bromooctane, MeOH; (iii) Br_2, dichloromethane, AcOH.

substitution of electronegative F atoms enhances the device performance without increment in the torsional angle along the conjugated backbone through noncovalent attractive interactions with enhanced interchain ordering and improved carrier mobility.[12,18] Despite the above-mentioned chemical versatility of the benzotriazole unit, efficient PFETs have not been realized based on benzotriazole-based polymers, showing a hole mobility less than $\sim 10^{-2}$ $cm^2/(V{\cdot}s)$.[19,20] The molecular structural optimization of solution-processable semicrystalline conjugated polymers is needed to maximize the charge carrier mobility along with thermal, oxidational, and temporal device stability.

In this study, three functionalized benzotriazole units (N-alkyl benzotriazole (BTz), fluorinated (BTz-F), and alkoxy substituted (BTz-OR)) were synthesized as an electron-deficient building block to examine the structure−property relationships of the benzotriazole-based polymers for PFET applications (Scheme 1). The thiophene moiety was coupled with three BTz units as an electron-rich building block to yield three different types of D−A copolymers. By attaching a bulky side chain to the nitrogen atom of benzotriazole, the resulting polymers were readily soluble in common organic solvents without the need for alkyl or alkoxy substitution on the electron-rich thiophene moiety. Fluorine atom (Pauling electronegativity of 4.0 and diameter ~1.35 Å) substitution on BTz showed highly efficient PFET performance by virtue of the planar polymeric backbone and effective interchain ordering through noncovalent, intra- and interchain F···S, F···H−C, and C−F···π_F interactions[21,22] as well as by lowering both the highest occupied molecular orbital (HOMO) and lowest unoccupied molecular orbital (LUMO) levels simultaneously.[23] Alkoxy substitution on the electron-deficient acceptor unit is also a useful strategy for minimizing the dihedral angle through noncovalent S···O interaction (as well as N···H−C in Scheme 1b)[24−27] and imparting solubility without increasing the HOMO level.[28] Chemical modifications of the benzotriazole unit with fluorine or alkoxy substituents are expected to deliver effective polymer packing and the charge carrier mobility with oxidational stability. A fluorinated BTz-F and thiophene containing polymer (**PTBTz-F**) showed a ~3 orders of magnitude higher hole mobility (μ_h = 1.9 $cm^2/(V{\cdot}s)$, on/off ratio = 8×10^7) with pronounced thermal stability compared to the nonfluorinated one. Similarly, alkoxy substitution on the benzotriazole unit also enhanced the hole mobility ~3 fold (μ_h = 0.019 $cm^2/(V{\cdot}s)$) relative to that of the unsubstituted one. Atomic force microscopy (AFM) and X-ray diffraction (XRD) measurements revealed clear correlations of the chemical structure modification with the molecular packing, film morphology, and resulting PFET properties.

EXPERIMENTAL SECTION

Materials. All chemical reagents were purchased from Aldrich, Tokyo Chemical Industry, and Junsei Chemical and used without

dx.doi.org/10.1021/cm4042346 | Chem. Mater. 2014, 26, 2147−2154

further purification. 2-Hexyldecylbromide,[29] 2,5-bis(trimethylstannyl)-thiophene,[30] 4,5-bis(octyloxy)-benzene-1,2-diammonium chloride,[31] and 5,6-difluoro-1H-benzo[d][1,2,3]triazole[32] were synthesized by following the previous literature procedures. The intermediates and monomers (BTz, BTz-F) were prepared by modifying the previously reported procedures.[14,33]

5,6-Bis(octyloxy)-1H-benzo[d][1,2,3]triazole (1). In a cooled ice bath, 4,5-bis(octyloxy)benzene-1,2-diammonium chloride (5.13 g, 11.7 mmol) was dissolved in 150 mL of acetic acid. $NaNO_2$ (8.35 g, 121 mmol) in 15 mL of H_2O was added into the above mixture and stirred for 10 min. The color of solution changed immediately into green, then red. The mixture was stirred overnight at 85 °C and cooled down to room temperature. The reaction mixture was extracted with chloroform, washed with water, and dried over anhydrous $MgSO_4$. The solution was concentrated under reduced pressure, and the crude compound was purified by silica gel column chromatography (eluent, petroleum ether:ethyl acetate = 1:1 by volume) to give a white solid. Yield: 3.99 g (90.8%). ^{1}H NMR (300 MHz, $CDCl_3$, ppm): δ 7.19 (s, 2H), 4.01 (t, 4H), 1.85 (quin) 1.47 (m, 4H), 1.26 (m, 16H), 0.87 (t, 6H). ^{13}C NMR (75 MHz, $CDCl_3$, ppm): δ 150.19, 134.14, 95.45, 69.19, 31.76, 29.35, 29.23, 28.92, 26.00, 22.63, 14.07. Anal. Calcd for $C_{22}H_{37}N_3O_2$: C, 70.36; H, 9.93; N, 11.19. Found: C, 70.14; H, 10.12; N, 11.11.

2-Octyl-5,6-bis(octyloxy)-2H-benzo[d][1,2,3]triazole (2). Compound **1** (1.26 g, 3.35 mmol), potassium *tert*-butoxide (1.52 g, 13.5 mmol), and 1-bromooctane (2.61 g, 13.5 mmol) were dissolved in methanol (30 mL). The reaction mixture was refluxed at 80 °C overnight. After removal of the solvent, the residue was dissolved in chloroform and washed with water. The organic layer was dried over $MgSO_4$ and concentrated under reduced pressure. The crude compound was purified by silica gel column chromatography (eluent, petroleum ether:dichloromethane = 1:1 by volume) to give a white solid. Yield: 0.7 g (42.8%). ^{1}H NMR (300 MHz, $CDCl_3$, ppm): δ 7.05 (s, 2H), 4.59 (t, 2H), 4.04 (t, 4H), 2.05 (m, 2H), 1.88 (quin, 4H), 1.62 (m. 2H), 1.51 (m, 4H), 1.29 (m, 24H), 0.87 (m, 9H). ^{13}C NMR (75 MHz, $CDCl_3$, ppm): δ 150.89, 139.73, 96.34, 68.90, 55.89, 31.78, 31.70, 30.09, 29.35, 29.26, 29.01, 28.87, 26.55, 26.03, 22.65, 22.58, 14.09. Anal. Calcd for $C_{30}H_{53}N_3O_2$: C, 73.87; H, 10.95; N, 8.61. Found: C, 74.07; H, 11.24; N, 8.52.

4,7-Dibromo-2-octyl-5,6-bis(octyloxy)-2H-benzo[d][1,2,3] triazole (BTz-OR). To a solution of compound **2** (2.44 g, 5 mmol) in a mixture of dichloromethane (100 mL) and acetic acid (60 mL) was added bromine (1.85 mL, 36 mmol), and the resulting mixture was stirred in the dark for 48 h at room temperature. The mixture was then quenched by adding aq. $NaHSO_3$ (sat.) solution, extracted with dichloromethane, and washed with water, aq. $NaHCO_3$ (sat.), and 1 M Na_2SO_3 solution. The organic layer was dried over $MgSO_4$ and concentrated under reduced pressure. The crude product was purified by silica gel column chromatography (eluent, petroleum ether:-dichloromethane = 4:1 by volume) to give colorless oil. Yield: 2.26 g (76.0%). ^{1}H NMR (300 MHz, $CDCl_3$, ppm): δ 4.71 (t, 2H), 4.08 (t, 4H), 2.11 (m, 2H), 1.86 (quin, 4H), 1.55 (m, 6H), 1.30 (m, 24H), 0.87 (m, 9H). ^{13}C NMR (75 MHz, $CDCl_3$, ppm): δ 151.36, 140.49, 102.97, 74.84, 74.78, 74.71, 57.11, 31.80, 31.66, 30.25, 30.20, 29.40, 29.26, 28.98, 28.92, 26.45, 26.00, 22.64, 22.56, 14.14, 14.10, 14.05. Anal. Calcd for $C_{30}H_{51}Br_2N_3O_2$: C, 55.82; H, 7.96; N, 6.51. Found: C, 56.06; H, 8.20; N, 6.41.

Poly[2-(2-hexyldecyl)-4-(thiophen-2-yl)-2H-benzo[d] [1,2,3]-triazole] (PTBTz). 2,5-Bis(trimethylstannyl)thiophene (400 mg, 0.976 mmol), BTz (489 mg, 0.976 mmol), $Pd_2(dba)_3$ (26.8 mg, 29.3 μmol), and tri(o-tolyl)phosphine (35.6 mg, 117.1 μmol) were dissolved in dry chlorobenzene (4.9 mL). The mixture was heated at 100 °C for 5 min, 120 °C for 5 min, 140 °C for 5 min, and 170 °C for 60 min in a microwave reactor. 2-Bromothiophene (1 equiv.) and 2-(tributylstannyl)thiophene (2 equiv.) were sequentially added to the reaction mixture as an end-capper and heated at 170 °C for 10 min. The reaction mixture was allowed to cool down to room temperature and then precipitated into a MeOH/HCl mixture (250 mL/10 mL). The polymer was filtered and purified by Soxhlet extraction in acetone (12 h) and in n-hexane (12 h). The n-hexane fraction was precipitated into MeOH and recovered by filtration. The final product was obtained after drying under vacuum at 50 °C. Yield: 290 mg (69.8%). ^{1}H NMR (300 MHz, $CDCl_3$, ppm): δ 8.08 (br, 2H), 7.25 (br, 2H), 4.73 (br, 2H), 2.34 (br, 1H), 1.29 (br, 24H), 0.87 (br, 6H). Number-average molecular weight (GPC, eluent = $C_6H_4Cl_2$): M_n = 7 kDa (PDI = 2.00).

Poly[2-(2-hexyldecyl)-5,6-difluoro-4-(thiophen-2-yl)-2H-benzo[d][1,2,3]triazole] (PTBTz-F). 2,5-Bis(trimethylstannyl)-thiophene (277 mg, 0.676 mmol), BTz-F (363 mg, 0.676 mmol), $Pd_2(dba)_3$ (18.6 mg, 20.3 μmol), and tri(o-tolyl)phosphine (24.7 mg, 81.1 μmol) were dissolved in dry chlorobenzene (4 mL). **PTBTZ-F** was synthesized by following the similar procedure as for **PTBTz**. The polymer was purified by Soxhlet extraction in acetone (12 h), in n-hexane (12 h), and in chloroform (6 h). The chloroform fraction was precipitated into MeOH and recovered by filtration. Yield: 240 mg (76.9%). ^{1}H NMR (300 MHz, $CDCl_3$, ppm): δ 7.96 (br, 2H), 4.78 (br, 2H), 2.40 (br, 1H), 1.40 (br, 24H), 0.89 (br, 6H). Number-average molecular weight (GPC, eluent = $C_6H_4Cl_2$): M_n = 7.5 kDa (PDI = 1.19).

Poly[2-octyl-5,6-bis(octyloxy)-4-(thiophen-2-yl)-2H-benzo-[d][1,2,3]triazole] (PTBTz-OR). 2,5-Bis(trimethylstannyl)thiophene (327 mg, 0.799 mmol), BTz-OR (516 mg, 0.799 mmol), $Pd_2(dba)_3$ (21.9 mg, 24.0 μmol), and tri(o-tolyl)phosphine (29.2 mg, 95.9 μmol) were dissolved in dry toluene (4 mL). **PTBTZ-OR** was synthesized by following the similar procedure as for **PTBTz**. The polymer was purified by Soxhlet extraction in acetone (12 h), in n-hexane (12 h), and in chloroform (6 h). The chloroform fraction was precipitated into MeOH and recovered by filtration. Yield: 408 mg (89.6%). ^{1}H NMR (300 MHz, $CDCl_3$, ppm): δ 8.61 (br, 2H), 4.82 (br, 2H), 4.25 (br, 4H), 2.26 (br, 2H), 2.14 (br, 4H), 1.30 (br, 30H), 0.87 (t, 9H). Number-average molecular weight (GPC, eluent = $C_6H_4Cl_2$): M_n = 35 kDa (PDI = 2.21).

Measurements. ^{1}H and ^{13}C NMR spectra were recorded on a JEOL (JNM-AL300) FT NMR system operating at 300 and 75 MHz, respectively. Elemental analysis was performed at Korea Polymer Testing and Research Institute, Korea. The polymerization reaction was done by using a microwave reactor (Biotage Initiator). The number- and weight- average molecular weights of the polymers were determined relative to polystyrene standards with *o*-dichlorobenzene as the eluent at 80 °C using a gel permeation chromatography (GPC) system equipped with a Waters 1515 isocratic HPLC pump, a temperature control module, and a Waters 2414 refractive index detector. Thermogravimetric analysis (TGA) and differential scanning calorimetry (DSC) measurements of the polymers were performed using a TA Instruments TGA 2050 thermogravimetric analyzer and DSC Q200 under a nitrogen atmosphere at a heating and cooling rate of 10 °C/min. UV−vis absorption spectra were measured using a Jasco (V-630) spectrophotometer. Cyclic voltammetry data were measured on a Versa STAT 3 (Princeton Applied Research) with a three-electrode cell in 0.1 M tetrabutylammonium tetrafluoroborate (Bu_4NBF_4) in CH_3CN at a scan rate of 50 mV/s. A platinum electrode coated with a thin polymer film was used as the working electrode, and platinum and $Ag/AgNO_3$ electrodes were used as the counter- and reference electrodes, respectively. All measurements were calibrated against an internal standard of ferrocene (Fc), the ionization potential (IP) value of which was assumed to be −4.78 V for the Fc/Fc^+ redox system. The thickness of polymer films was measured using ellipsometry. Atomic force microscopy (AFM, Multimode IIIa, Digital Instruments) was operated in a tapping mode to acquire the surface images of polymer films. X-ray diffraction (XRD) studies were performed at the 5A beamline at the Pohang Accelerator Laboratory (PAL), Korea. To predict the structural geometry of the polymers, density functional theory (DFT) calculations of simplified molecular structures were performed (B3LYP/6-31G** level).

PFET Fabrication. Electrical properties of the BTz-based polymers were characterized in a top-contact PFET configuration using a 300 nm thick SiO_2 dielectric on a highly doped n-Si substrate, which served as the gate electrode. The substrate was cleaned with piranha solution and ozone-treated for 20 min. Cleaned substrates were treated with octadecyltrichlorosilane (ODTS) in toluene for 90 min at room

temperature, and the semiconducting polymer films were spin-coated at 6000 rpm from a 0.2 wt % chloroform solution (thickness ~40 nm). Gold source and drain electrodes (thickness ~100 nm) were evaporated on top of the semiconductor layer using a shadow mask. For all measurements, the channel length (L) and width (W) were 160 μm and 1,600 μm, respectively. The PFET devices were annealed at various temperatures for 10 min under a nitrogen atmosphere. Based on the UV−vis spectral changes vs annealing temperature, the XRD and PFET device characteristics were investigated in different temperature ranges for the polymers. The electrical characteristics of the PFETs were measured using Keithley 2400 and 236 source/measure units under ambient condition. Field-effect mobility was extracted in the saturation regime from the slope of the source−drain current, wherein the slope of a plot of square root of the drain current versus gate voltage (V_G) was fit to the following equation: $I_{DS} = (WC_i/2L)\mu(V_G - V_{th})^2$, where I_{DS} is the drain current, C_i is the capacitance per unit area of dielectric, μ is the field-effect mobility, and V_{th} is the threshold voltage.

RESULTS AND DISCUSSION

Molecular Design and Synthesis. Three different benzotriazole-based copolymers were designed and synthesized, as shown in Scheme 1. The electron-deficient benzotriazole unit was chosen as a building block because the benzotriazole unit can be functionalized at the 2(N) and 5, 6(C) positions, through which the solution processability and the physical, optical, and electronic properties of the resulting polymers can be fine-tuned easily. The central nitrogen atom can be alkylated to achieve solution processability, and other substituents (such as fluoro and alkoxy groups) can be also introduced at the 5- and 6-positions (on the benzene ring), modulating the frontier orbital levels and inter- and/or intrachain interactions. 2-Hexyldecyl- or n-octyl side chains were introduced at the central nitrogen atom to resolve the solubility issues. As shown in Scheme S1, BTz[33] and BTz-F[14] were synthesized by modifying the previously reported procedures. For the synthesis of the alkoxy-substituted BTz-OR, 4,5-bis(octyloxy)-benzene-1,2-diammonium chloride was reacted with $NaNO_2$ to produce compound **1** in ~91% yield. Successive alkylation resulted in a mixture of N-alkylated compounds due to the lack of regioselectivity among the three N atoms (~43% yield). Finally, bromination of compound **2** successfully yielded the monomer, BTz-OR (76% yield). Three types of BTz monomers (BTz, BTz-F, BTz-OR) were reacted with 2,5-bis(trimethylstannyl)thiophene under Stille coupling polymerization conditions (in 70−90% yield) using $Pd_2(dba)_3$/P(*o*-tol)$_3$ as a catalyst, yielding three different BTz-based copolymers, poly[2-(2-hexyldecyl)-4-(thiophen-2-yl)-2H-benzo[d][1,2,3]triazole] (**PTBTz**), poly[2-(2-hexyldecyl)-5,6-difluoro-4-(thiophen-2-yl)-2H-benzo[d][1,2,3]triazole] (**PTBTz-F**), and poly[2-octyl-5,6-bis(octyloxy)-4-(thiophen-2-yl)-2H-benzo[d][1,2,3]triazole] (**PTBTz-OR**).

Fluoro- or alkoxy substituents were introduced to the BTz unit to modulate the intra-, interchain interactions and the resulting semicrystalline orientation of the polymers. In fluorinated **PTBTz-F**, noncovalent attractive interactions via intra- and/or interchain F···S, F···H−C, and C−F···π_F interactions[21] (as well as N···H−C) are likely to induce strong intermolecular ordering. Similarly, the alkoxy-substituted **PTBTz-OR** polymer exhibited an almost planar structure via noncovalent coulomb interactions between the partially positive S (δ^+) and negative O (δ^-) atoms in the polymer chain (Scheme 1).[28] The noncovalent coulomb interactions have been well documented previously. Guo et al. emphasized the noncovalent attractive interactions (by virtue of S···O) to fix the chain conformation and planarity for the methoxy-substituted thiophene and bithiazole compounds.[27] Wang et al. also reported the S···F interaction controls the stacking orientation in fluorinated benzobisbenzothiophenes by single-crystal X-ray analyses.[34] Recently, Marks and Facchetti groups also emphasized that the weak conformational lock plays an important role to achieve well-ordered film morphology and high carrier mobility.[26,27] Ratner et al. reported that how various nonbonding interactions would affect conformation of conjugated polymers and small molecules by way of conformational locking, where the binding energy was calculated for several nonbonding interactions. The binding energy of CH···N, O···S, and F···S interactions was estimated to be 2.2, 0.51, and 0.44 kcal/mol, respectively.[17] Computational studies using density functional theory were performed for the BTz polymers. The detailed torsional profiles for the three polymers are shown in Figure S1. **PTBTz-OR** shows a torsional angle of ~10°, emphasizing the intramolecular noncovalent S···O attractive interactions. The introduction of fluorine atoms on BTz decreases the torsional angle (~0°) in **PTBTz-F** further due to the intrachain C−F···S coulomb interactions and the small van der Waals radius of the F atom. The energy barrier for the two energy minimum conformations was estimated to be 4.7, 5.2, and 5.2 kcal/mol for **PTBTz**, **PTBTz-F**, and **PTBTz-OR**, respectively. This can be interpreted in terms of the additional stabilization (by ~0.5 kcal/mol) of **PTBTz-F** and **PTBTz-OR** with noncovalent attractive interactions by way of S···F and S···O interactions, etc. The additional attractive interactions enhance the backbone planarity with conformational lock, although additional substituents may increase a steric repulsion with compared to **PTBTz**. The planar polymer backbone is beneficial to increase the interchain ordering. In addition, the intermolecular S···F and S···O attractive interactions can induce a tighter interchain packing. The resulting chain-ordering behavior and device properties were compared with those of the unsubstituted **PTBTz**. All the polymers were readily soluble in chlorinated organic solvents, i.e. chlorinated benzene and chloroform, etc. The molecular weight of the polymers was measured in the range of 7−35 kDa by GPC relative to a polystyrene standard. All polymers showed good thermal stability up to 330−450 °C. Alkoxy-substituted **PTBTz-OR** exhibited a relatively lower decomposition temperature (T_d) of approximately 330 °C due to break up of the alkoxy side chains. No clear phase transitions were observed for all polymers in the DSC measurements up to 280 °C (Figure S2).

Optical and Electrochemical Properties. Figure 1 shows the normalized absorption spectra of the BTz-based polymers in solution and film before and after thermal annealing. All the polymers showed similar absorption spectra in a range of 400−700 nm due to the strong intramolecular charge transfer (ICT) interactions from thiophene to the BTz moieties.[35] The optical band gap was determined to be 1.87−1.97 eV from the onset of the spectra in the film. The absorption spectra of the BTz-based polymers in the thin film were red-shifted (by ca. 20−40 nm) with a substantially enhanced vibronic shoulder peak at ~600 nm, compared to those in solution, suggesting extended π-conjugation via intermolecular organization in the solid state (Table 1). Upon annealing, the shoulder peak was intensified, indicating pronounced intermolecular interactions with tight interchain packing (or aggregation) in the film via thermal

dx.doi.org/10.1021/cm4042346 | Chem. Mater. 2014, 26, 2147−2154

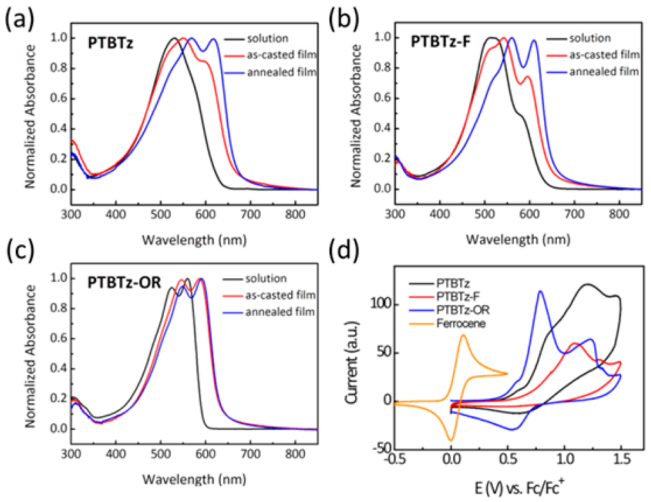

Figure 1. Normalized UV−vis absorption spectra in solution and in thin film before and after thermal annealing. (a) **PTBTz**, (b) **PTBTz-F**, and (c) **PTBTz-OR**. (d) Cyclic voltammogram for polymers.

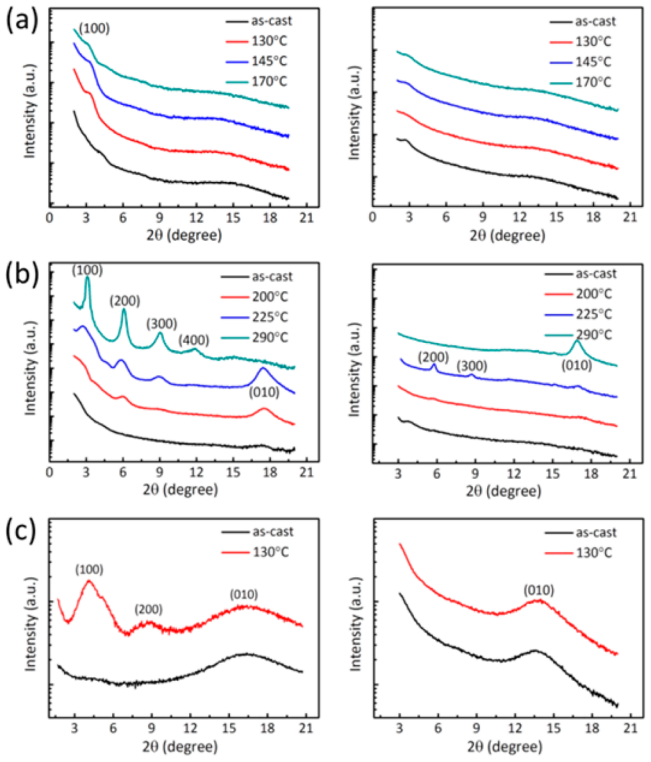

Figure 2. Out-of-plane (left) and in-plane (right) X-ray diffraction of (a) **PTBTz**, (b) **PTBTz-F**, and (c) **PTBTz-OR** films with changing annealing temperatures.

treatments. The most pronounced shoulder peak was observed for **PTBTz-F**.

Cyclic voltammetry of all polymers in the film was performed to estimate their frontier orbital energy levels (Figure 1, Table 1). All the polymers showed a strong oxidative peak, but no reductive peak was observed, indicating pronounced p-type characteristics. The estimated HOMO level for **PTBTz**, **PTBTz-F**, and **PTBTz-OR** was −5.24, −5.36, and −5.20 eV, respectively. The calculated LUMO level for **PTBTz**, **PTBTz-F**, and **PTBTz-OR** was −3.37, −3.44, and −3.23 eV, respectively, from the HOMO level and its optical band gap ($E_{LUMO} = E_{HOMO} + E_g^{opt}$). Fluorination on the BTz unit stabilizes both the HOMO and LUMO levels due to the strong inductive effect of fluorine atoms, thereby improving the oxidational stability of the resulting polymeric structure (**PTBTz-F**).[23] Alkoxy substitution on the BTz unit increased the HOMO and LUMO levels slightly compared to unsubstituted **PTBTz**. The frontier orbital structures calculated by DFT showed that the HOMO was delocalized on both thiophene and BTz moieties, and the LUMO was concentrated mainly on BTz (Figure S3).

Thin-Film Structure and Morphology. X-ray diffraction (XRD) was used to examine the molecular ordering in the thin films. The chloroform solution (0.2 wt %) of each polymer was spin-casted on top of the ODTS-treated SiO_2/Si substrate. Figure 2 shows the XRD patterns of the polymer films at different annealing temperatures. The as-cast **PTBTz** film showed no discernible diffraction peak in both the out-of-plane and in-plane directions. After annealing at 130 °C, a weak (100) XRD peak along the out-of-plane direction was observed with a *d*-spacing of 18.72 Å. With increasing annealing temperature, the intensity of the (100) peak decreased slightly. In contrast, **PTBTz-F** showed drastic changes in molecular packing with the thermal treatments, where no XRD pattern was observed in the pristine film. On the other hand, thermal annealing induced the intermolecular orientation with intensified scattering peaks.

The film annealed at 225 °C showed three diffraction (100), (200), (300) peaks along both the out-of-plane and in-plane directions with the corresponding $\pi-\pi$ stacking (010) peaks in both directions ($d_{(010)}$ = 3.62 Å), indicating an isotropic (mixed face-on and edge-on) interchain orientation. Thermal treatment at 290 °C induced more defined and intensified XRD peaks along the out-of-plane direction (2θ = 3.08°, 6.08°, 9.04°, and 11.84°, $d_{(100)}$ = 19.94 Å) and a clear $\pi-\pi$ stacking peak (2θ = 16.9°, $d_{(010)}$ = 3.65 Å) along the in-plane direction, indicating the presence of highly ordered lamellar sheets perpendicular to the substrate as well as the preferential formation of edge-on oriented polymer stacks[36,37] These well-ordered molecular

Table 1. Physical, Thermal, Optical, and Electrochemical Properties of Polymers

polymer	M_n[a] (kDa)/PDI[b]	T_d[c] (°C)	λ_{max} (in soln)	λ_{max} (in film)[d]	λ_{max} (annealed)[f]	E_g^{opt} (eV)[g]	HOMO (eV)[h]	LUMO (eV)[i]
PTBTz	7/2.00	419	531	550, 599 (s)[e]	568, 617	1.87	−5.24	−3.37
PTBTz-F	7.5/1.19	453	516	542, 595	560, 610	1.92	−5.36	−3.44
PTBTz-OR	35/2.21	336	525, 560	541, 587	548, 590	1.97	−5.20	−3.23

[a]Number-average molecular weight. [b]Polydispersity index. [c]Decomposition temperature with 5% weight loss. [d]Films were spin-casted from a 1 wt % chloroform solution for 30 s at 1500 rpm. [e]s in parentheses indicates the shoulder peak. [f]Annealed film at the temperature showing the best PFET performance. [g]Optical band gap was estimated from the absorption onset in film. [h]The HOMO level was estimated from the first oxidation potential relative to the ferrocene/ferrocenium (Fc/Fc^+) system. [i]The LUMO level was calculated using the HOMO energy level and optical band gap ($E_{LUMO} = E_{HOMO} + E_g^{opt}$).

dx.doi.org/10.1021/cm4042346 | *Chem. Mater.* 2014, 26, 2147−2154

structures facilitate efficient lateral charge transport along the π stacks in the PFET architecture.[38] Enhanced molecular ordering was also observed in the **PTBTz-OR** film by thermal annealing at 130 °C, where the out-of-plane scattering peaks were measured with the $\pi-\pi$ stacking (010) peak ($d_{(010)}$ = 4.46 Å) in the in-plane direction, indicating the preferential formation of the edge-on orientation. The semicrystalline characteristics in the XRD patterns are consistent with those obtained from UV−visible absorption spectroscopy (Figure 1, S4). The enhanced planarity, intra- and intermolecular interactions upon fluorination improved the molecular ordering with a highly ordered nanoscale morphology. Alkoxy side-chain substitution also promoted molecular ordering through noncovalent coulomb interactions between the S (δ^+) and O (δ^-) atoms. Atomic force microscopy (AFM) in tapping mode was carried out to examine the morphology of the as-cast and annealed films. Figure S5 shows the surface morphology and root-mean-square (rms) roughness of the BTz-based polymers. Before the thermal treatments, the pristine films of the three polymers showed a smooth morphology without crystalline features. Thermal annealing clearly induced morphological changes with an increase in the rms roughness, possibly due to polymer self-organization to form ordered domains, as indicated by XRD measurements.

PFET Properties. To correlate the temperature-dependent changes in the film morphology with the charge carrier mobility, PFET devices were fabricated, and the I−V characteristics were investigated for the BTz-based polymers. Table 2 lists the extracted electrical parameters of PFET devices. As shown in Figure 3, the typical p-type transfer characteristics were measured for all the polymers where the thermal annealing treatments substantially improved the hole mobility, being consistent with the data in the UV−vis and XRD measurements. The measured field-effect mobility of the as-cast **PTBTz** and **PTBTz-OR** films was 5.8×10^{-6} $cm^2/(V{\cdot}s)$ and 9.1×10^{-4} $cm^2/(V{\cdot}s)$, respectively. Thermal annealing resulted in 2−3 orders of magnitude improvement in the hole mobility, up to 7.0×10^{-3} $cm^2/(V{\cdot}s)$ for **PTBTz** (annealed at 145 °C) and 1.9×10^{-2} $cm^2/(V{\cdot}s)$ for **PTBTz-OR** (annealed at 130 °C). The on/off ratio also improved substantially after the thermal treatments ($7 \times 10^2 \rightarrow 3 \times 10^6$ for **PTBTz**, $1 \times 10^5 \rightarrow 4 \times 10^5$ for **PTBTz-OR**). In the case of fluorine-substituted **PTBTz-F**, the PFET mobility of 2.6×10^{-5} $cm^2/(V{\cdot}s)$ was measured before thermal annealing. With increasing annealing temperature, the hole mobility was enhanced dramatically, showing the maximum mobility of 1.9 $cm^2/(V{\cdot}s)$ (by annealing at 305 °C) with a high on/off ratio (8×10^7). This showed a good agreement with the XRD data, showing predominant edge-on lamellar packing with tight $\pi-\pi$ stacking (3.65 Å). Compared to the unsubstituted **PTBTz**, the alkoxy and fluorine substituted polymers showed substantially improved carrier transport properties (by 1 to 3 orders compared to that of **PTBTz**), which is closely related to the enhanced interchain ordering by noncovalent intra- and interchain interactions via F···S, F···H−C, C−F···π_F (for **PTBTz-F**), or S···O (for **PTBTz-OR**) as well as the N···H−C interactions.

A pronounced difference in the field-effect mobility was observed by chemical modification of the BTz moiety. The order of the hole mobility is as follows: **PTBTz-F** (1.9 $cm^2/(V{\cdot}s)$) > **PTBTz-OR** (0.019 $cm^2/(V{\cdot}s)$) > **PTBTz** (7.0×10^{-3} $cm^2/(V{\cdot}s)$). The introduction of fluorine or alkoxy substituents onto the BTz unit enhances the intermolecular interactions of the polymeric chain, forming a semicrystalline structure upon thermal annealing. In particular, electronegative fluoro substituents decreased the energy levels of frontier orbitals substantially (see Table 1), which can improve the oxidational stability of the active material in organic optoelectronic devices.

Table 2. PFET Characteristics of BTz-Based Copolymers

polymer	T_a[a] (°C)	μ_h ($cm^2/(V{\cdot}s)$)	I_{on}/I_{off}	V_{th} (V)
PTBTz	as-cast	5.8×10^{-6}	7×10^2	−5.2
	130	6.9×10^{-3}	6×10^5	−20
	145	7.0×10^{-3}	3×10^6	−20
	170	6.5×10^{-3}	5×10^5	−21
	180	2.7×10^{-3}	3×10^5	−24
PTBTz-F	as-cast	2.6×10^{-5}	1×10^2	−4.2
	180	2.0×10^{-5}	7×10^4	−9.6
	200	0.34	2×10^7	−16
	240	0.36	8×10^7	−12
	290	1.5	3×10^7	−10
	305	1.9	8×10^7	−12
	320	0.57	2×10^7	−12
PTBTz-OR	as-cast	9.1×10^{-4}	1×10^5	−2.1
	105	5.1×10^{-3}	3×10^5	1.6
	130	1.9×10^{-2}	4×10^5	1.3
	145	1.0×10^{-2}	7×10^4	1.8
	170	1.6×10^{-4}	1×10^4	1.0

[a]Annealing temperature.

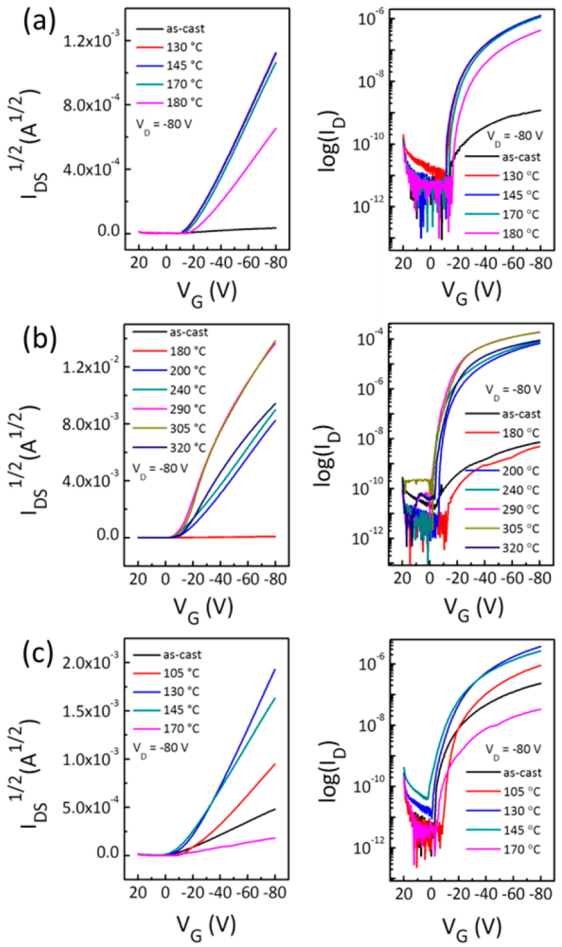

Figure 3. Transfer characteristics of (a) **PTBTz**, (b) **PTBTz-F**, and (c) **PTBTz-OR**-based PFET devices.

dx.doi.org/10.1021/cm4042346 | *Chem. Mater.* 2014, 26, 2147−2154

The thermal stability was also improved remarkably with fluorine substituents (T_d 453 °C) compared to unsubstituted **PTBTz** (T_d 419 °C). In addition, the electron-poor benzotriazole moiety can be alkylated on the central N atom for solution processability without attaching alkyl side-chains to thiophene. The alkylation of electron-rich thiophene increases the HOMO level and deteriorates the oxidational stability. The fluorinated and/or alkoxy substituted benzotriazole moiety has potential as a building block for optoelectronic polymeric structures, showing high thermal and oxidational stability as well as high device performance.

■ CONCLUSIONS

Thiophene and benzotriazole-based D−A type planar π-conjugated copolymers were designed and synthesized. The chemically versatile BTz unit not only endows solution processability without deteriorating the π-backbone planarity but also gives rise to functional sites that can incorporate other substituents to modulate the photophysical, frontier orbital levels and oxidational stability. A conformational lock through noncovalent attractive interactions between the electronegative element (F or O) and adjacent sulfur (δ^+) on thiophene induces favorable molecular ordering, which is essential to realizing high performance PFETs. The fluorinated polymer, **PTBTz-F**, showed high thermal stability (T_d 453 °C) and formed a highly ordered structure after thermal annealing with a preferred edge-on orientation. **PTBTz-F** enhanced hole mobility substantially up to 1.9 $cm^2/(V{\cdot}s)$. In addition, the alkoxy-substituted **PTBTz-OR** showed an enhanced hole mobility of 0.019 $cm^2/(V{\cdot}s)$. The fluorinated and/or alkoxy-substituted benzotriazole units may be versatile building blocks for organic optoelectronic devices by allowing easy tuning of the interchain ordering, charge carrier mobility, and thermal- and oxidational stability of the resulting π-conjugated photoactive materials.

■ ASSOCIATED CONTENT

Ⓢ Supporting Information

Synthesis and characterization of intermediates, TGA/DSC thermograms, calculated HOMO and LUMO structures, UV−vis absorption spectra of annealed films, and AFM images for the BTz-based polymers. This material is available free of charge via the Internet at http://pubs.acs.org.

■ AUTHOR INFORMATION

Corresponding Authors

*E-mail: cep@postech.ac.kr (C.E.P.).
*E-mail: hywoo@pusan.ac.kr (H.Y.W.).

Author Contributions

[Δ]Yum, An, and Wang contributed equally.

Notes

The authors declare no competing financial interest.

■ ACKNOWLEDGMENTS

This study was supported by the National Research Foundation (NRF) Grant, Korea (2012R1A1A2005855, 2013M3C1A3065522, NRF-2009-0079630). This work was supported by a grant (No. 2011-0031639) from the Center for Advanced Soft Electronics under the Global Frontier Research Program of the Ministry of Education, Science and Technology, Korea. This work was also supported by New and Renewable Energy Program of the Korea Institute of Energy Technology Evaluation and Planning (KETEP) funded by the Korea government Ministry of Trade, industry & Energy (20113010010030). Synchrotron X-ray scattering measurements at Pohang Accelarator Laboratory were supported by MEST, POSCO, and POSTECH Foundation.

■ REFERENCES

(1) Kang, I.; An, T. K.; Hong, J. A.; Yun, H. J.; Kim, R.; Chung, D. S.; Park, C. E.; Kim, Y. H.; Kwon, S. K. *Adv. Mater.* **2013**, *25*, 524.
(2) Baeg, K. J.; Khim, D.; Kim, J.; Yang, B. D.; Kang, M.; Jung, S. W.; You, I. K.; Kim, D. Y.; Noh, Y. Y. *Adv. Funct. Mater.* **2012**, *22*, 2915.
(3) Arias, A. C.; Ready, S. E.; Lujan, R.; Wong, W. S.; Paul, K. E.; Salleo, A.; Chabinyc, M. L.; Apte, R.; Street, R. A.; Wu, Y.; Liu, P.; Ong, B. *Appl. Phys. Lett.* **2004**, *85*, 3304.
(4) Tsao, H. N.; Cho, D. M.; Park, I.; Hansen, M. R.; Mavrinskiy, A.; Yoon, D. Y.; Graf, R.; Pisula, W.; Spiess, H. W.; Mullen, K. *J. Am. Chem. Soc.* **2011**, *133*, 2605.
(5) Chen, H. J.; Guo, Y. L.; Yu, G.; Zhao, Y.; Zhang, J.; Gao, D.; Liu, H. T.; Liu, Y. Q. *Adv. Mater.* **2012**, *24*, 4618.
(6) Lee, J.; Han, A. R.; Kim, J.; Kim, Y.; Oh, J. H.; Yang, C. *J. Am. Chem. Soc.* **2012**, *134*, 20713.
(7) Guo, X. G.; Ortiz, R. P.; Zheng, Y.; Kim, M. G.; Zhang, S. M.; Hu, Y.; Lu, G.; Facchetti, A.; Marks, T. J. *J. Am. Chem. Soc.* **2011**, *133*, 13685.
(8) Mei, J. G.; Kim, D. H.; Ayzner, A. L.; Toney, M. F.; Bao, Z. A. *J. Am. Chem. Soc.* **2011**, *133*, 20130.
(9) Ha, J. S.; Kim, K. H.; Choi, D. H. *J. Am. Chem. Soc.* **2011**, *133*, 10364.
(10) Yi, Z. R.; Sun, X. N.; Zhao, Y.; Guo, Y. L.; Chen, X. G.; Qin, J. G.; Yu, G.; Liu, Y. Q. *Chem. Mater.* **2012**, *24*, 4350.
(11) Lei, T.; Cao, Y.; Zhou, X.; Peng, Y.; Bian, J.; Pei, J. *Chem. Mater.* **2012**, *24*, 1762.
(12) Lei, T.; Dou, J. H.; Ma, Z. J.; Yao, C. H.; Liu, C. J.; Wang, J. Y.; Pei, J. *J. Am. Chem. Soc.* **2012**, *134*, 20025.
(13) Kang, I.; Yun, H.-J.; Chung, D. S.; Kwon, S.-K.; Kim, Y.-H. *J. Am. Chem. Soc.* **2013**, *135*, 14896.
(14) Price, S. C.; Stuart, A. C.; Yang, L. Q.; Zhou, H. X.; You, W. *J. Am. Chem. Soc.* **2011**, *133*, 4625.
(15) Min, J.; Zhang, Z. G.; Zhang, M. J.; Li, Y. F. *Polym. Chem.* **2013**, *4*, 1467.
(16) Min, J.; Zhang, Z. G.; Zhang, S. Y.; Li, Y. F. *Chem. Mater.* **2012**, *24*, 3247.
(17) Jackson, N. E.; Savoie, B. M.; Kohlstedt, K. L.; de la Cruz, M. O.; Schatz, G. C.; Chen, L. X.; Ratner, M. A. *J. Am. Chem. Soc.* **2013**, *135*, 10475.
(18) Zhou, H. X.; Yang, L. Q.; Stuart, A. C.; Price, S. C.; Liu, S. B.; You, W. *Angew. Chem., Int. Ed.* **2011**, *50*, 2995.
(19) Liu, B.; Chen, X. W.; He, Y. H.; Li, Y. F.; Xu, X. J.; Xiao, L.; Li, L. D.; Zou, Y. P. *J. Mater. Chem. A* **2013**, *1*, 570.
(20) Liu, X. P.; Zhang, J.; Tang, P.; Yu, G.; Zhang, Z. Y.; Chen, H. J.; Chen, Y.; Zhao, B.; Tan, S. T.; Shen, P. *Org. Electron.* **2012**, *13*, 1671.
(21) Reichenbacher, K.; Suss, H. I.; Hulliger, J. *Chem. Soc. Rev.* **2005**, *34*, 22.
(22) Okamoto, T.; Nakahara, K.; Saeki, A.; Seki, S.; Oh, J. H.; Akkerman, H. B.; Bao, Z. N.; Matsuo, Y. *Chem. Mater.* **2011**, *23*, 1646.
(23) Son, H. J.; Wang, W.; Xu, T.; Liang, Y. Y.; Wu, Y. E.; Li, G.; Yu, L. P. *J. Am. Chem. Soc.* **2011**, *133*, 1885.
(24) Zotti, G.; Gallazzi, M. C.; Zerbi, G.; Meille, S. V. *Synth. Met.* **1995**, *73*, 217.
(25) Meille, S. V.; Farina, A.; Bezziccheri, F.; Gallazzi, M. C. *Adv. Mater.* **1994**, *6*, 848.
(26) Huang, H.; Chen, Z. H.; Ortiz, R. P.; Newman, C.; Usta, H.; Lou, S.; Youn, J.; Noh, Y. Y.; Baeg, K. J.; Chen, L. X.; Facchetti, A.; Marks, T. J. *J. Am. Chem. Soc.* **2012**, *134*, 10966.
(27) Guo, X. G.; Quinn, J.; Chen, Z. H.; Usta, H.; Zheng, Y.; Xia, Y.; Hennek, J. W.; Ortiz, R. P.; Marks, T. J.; Facchetti, A. *J. Am. Chem. Soc.* **2013**, *135*, 1986.

(28) Lee, W.; Choi, H.; Hwang, S.; Kim, J. Y.; Woo, H. Y. *Chem.—Eur. J.* **2012**, *18*, 2551.
(29) Tylleman, B.; Gbabode, G.; Amato, C.; Buess-Herman, C.; Lemaur, V.; Cornil, J.; Aspe, R. G.; Geerts, Y. H.; Sergeyev, S. *Chem. Mater.* **2009**, *21*, 2789.
(30) Vanpham, C.; Macomber, R. S.; Mark, H. B.; Zimmer, H. *J. Org. Chem.* **1984**, *49*, 5250.
(31) Ding, P.; Chu, C. C.; Liu, B.; Peng, B.; Zou, Y. P.; He, Y. H.; Zhou, K. C.; Hsu, C. S. *Macromol. Chem. Phys.* **2010**, *211*, 2555.
(32) Charushin, V. N.; Kotovskaya, S. K.; Romanova, S. A.; Chupakhin, O. N.; Tomilov, Y. V.; Nefedov, O. M. *Mendeleev Commun.* **2005**, *15*, 45.
(33) Zhang, Z. H.; Peng, B.; Ding, P.; Liu, B.; He, Y. H.; Zhou, K. C.; Li, Y. F.; Pan, C. Y.; Zou, Y. P. *J. Appl. Polym. Sci.* **2011**, *120*, 2534.
(34) Wang, Y.; Parkin, S. R.; Gierschner, J.; Watson, M. D. *Org. Lett.* **2008**, *10*, 3307−3310.
(35) Banerji, N.; Gagnon, E.; Morgantin, P. Y.; Valouch, S.; Mohebbi, A. R.; Seo, J. H.; Leclerc, M.; Heeger, A. J. *J. Phys. Chem. C* **2012**, *116*, 11456.
(36) Rivnay, J.; Steyrleuthner, R.; Jimison, L. H.; Casadei, A.; Chen, Z. H.; Toney, M. F.; Facchetti, A.; Neher, D.; Salleo, A. *Macromolecules* **2011**, *44*, 5246.
(37) Choi, D.; Jin, S.; Lee, Y.; Kim, S. H.; Chung, D. S.; Hong, K.; Yang, C.; Jung, J.; Kim, J. K.; Ree, M.; Park, C. E. *ACS Appl. Mater. Interfaces* **2009**, *2*, 48.
(38) Joseph Kline, R.; McGehee, M. D.; Toney, M. F. *Nat. Mater.* **2006**, *5*, 222.